
Unsupervised Motion Representation Learning with Capsule Autoencoders

Ziwei Xu[†], Xudong Shen[‡], Yongkang Wong[†], Mohan Kankanhalli[†]

[†] School of Computing

[‡] NUS Graduate School

National University of Singapore

{ziwei-xu, mohan}@comp.nus.edu.sg

xudong.shen@u.nus.edu, yongkang.wong@nus.edu.sg

Abstract

We propose the Motion Capsule Autoencoder (MCAE), which addresses a key challenge in the unsupervised learning of motion representations: transformation invariance. MCAE models motion in a two-level hierarchy. In the lower level, a spatio-temporal motion signal is divided into short, local, and semantic-agnostic *snippets*. In the higher level, the snippets are aggregated to form full-length semantic-aware *segments*. For both levels, we represent motion with a set of learned transformation invariant templates and the corresponding geometric transformations by using capsule autoencoders of a novel design. This leads to a robust and efficient encoding of viewpoint changes. MCAE is evaluated on a novel Trajectory20 motion dataset and various real-world skeleton-based human action datasets. Notably, it achieves better results than baselines on Trajectory20 with considerably fewer parameters and state-of-the-art performance on the unsupervised skeleton-based action recognition task.

1 Introduction

Real-world movements contain a plethora of information beyond the literal sense of moving. For example, honeybees “dance” to communicate the location of a foraging site and human gait alone can reveal activities and identities [10]. Understanding these movements is vital for an artificial intelligent agent to comprehend and interact with the ever-changing world. Studies on social behavior analysis [8, 9], action recognition [63, 58], and video summarizing [59] have also acknowledged the importance of movement.

A key step towards understanding movements is to analyze their patterns. However, learning motion pattern representations is non-trivial due to (1) the curse of dimensionality from input data, (2) difficulties in modeling long-term dependencies in motion sequences, (3) high intra-class variation as a result of subject or viewpoint change, and (4) insufficient data annotation. The first two challenges have been ameliorated by the advances in keypoint detection, spatial-temporal feature extractors [38, 43, 50], and hierarchical temporal models [13, 56, 49]. The third and the fourth nonetheless remain hurdles and call for unsupervised transformation-invariant motion models.

Inspired by the viewpoint-invariant capsule-based representation for images [11, 17], we exploit capsule networks and introduce the Motion Capsule Autoencoder (MCAE), an unsupervised capsule framework that learns the transformation-invariant motion representation for keypoints. MCAE models motion signals in a two-level snippet-segment hierarchy. A snippet is a movement of a narrow time span, while a segment consists of multiple temporally-ordered snippets, representing a longer-time motion. In both the lower and the higher levels, the snippet capsules (SniCap) and the segment capsules (SegCap) maintain a set of templates as their identities—snippet templates and

segment templates, respectively—and transform them to reconstruct the input motion signal. While the snippet templates are explicitly modeled as motion sequences, the SegCaps are built upon the SniCaps and parameterize the segment templates *in terms of the snippet templates*, resulting in fewer parameters compared with single-layer modeling. The SniCaps and SegCaps learn transformation-invariant motion representation in their own time spans. The activations of the SegCaps serve as a high-level abstraction of the input motion signal.

The contributions of this work are as follows:

- We propose MCAE, an unsupervised capsule framework that learns a transformation-invariant, discriminative, and compact representation of motion signals. Two motion capsules are designed to generate representation at different abstraction levels. The lower-level representation captures the local short-time movements, which are then aggregated into higher-level representation that is discriminative for motion of wider time spans.
- We propose Trajectory20, a novel and challenging synthetic dataset with a wide class of motion patterns and controllable intra-class variations.
- Extensive experiments on both Trajectory20 and real-world skeleton human action datasets show the efficacy of MCAE. In addition, we perform ablation studies to examine the effect of different regularizers and some key hyperparameters of the proposed MCAE.

2 Related Works

Motion Representation A variety of methods have been proposed to learn (mostly human) motion representation from video frames [28, 3, 53, 23], depth maps [22, 47, 14, 37, 27], key-points/skeletons [4, 52, 21, 26, 57, 55, 24, 41, 29, 33], or point clouds [7, 6]. Earlier works use handcrafted features like Fourier coefficients [47], dense trajectory features [46, 30], and Lie group representations [44]. Some works use canonical human pose [32] or view-invariant short tracklets to learn robust feature for recognition [19]. The development of deep learning brings the usage of convolution networks (ConvNet) and recurrent networks for motion representation. Simonyan *et al.* [39] proposes a two-stream ConvNet which combines video frame with optical flow. C3D [43] proposes to use 3D convolution on the spatial-temporal cubes. Srivastava *et al.* [40] uses an LSTM-based encoder to map input frames to a fixed-length vector and apply task-dependent decoders for applications such as frame reconstruction and frame prediction. The combined use of convolution module and LSTM has also been proved effective in [38, 3, 51].

A series of works [48, 20, 18, 15, 45] have been proposed to address the problem of learning viewpoint-invariant motion representation from videos or keypoint sequences. MST-AOG [48] uses an AND-OR graph structure to separate appearance of mined parts from their geometry information. Li *et al.* [20] learn view-invariant representation by extrapolating cross-view motions. View-LSTM [18] defines a view decomposition, where the view-invariant component is learned by a Siamese architecture. While most of these works exploits multi-modal input of RGB frames, depth maps or keypoint trajectories, MCAE focuses on the pure keypoint motion.

Capsule Network MCAE is closely related to the Capsule Network [11], which is designed to represent objects in images using automatically discovered constituent parts and their poses. A capsule typically consists of a part identity, a set of transformation parameters (pose), and an activation. The explicit modeling of poses helps learning viewpoint-invariant part features that are more compact, flexible, and discriminative than traditional ConvNets. Capsules can be obtained via agreement-based routing mechanisms [34, 12]. More recently, Kosiorek *et al.* [17] proposed the unsupervised stacked capsule autoencoder (SCAE), which uses feed-forward encoders and decoders to learn capsule representations for images.

Apart from images, capsule network has been studied in other vision tasks. In [60, 61], capsule network is used for point cloud processing for 3D object classification and reconstruction. VideoCapsuleNet [5] proposes to generalize capsule networks from 2D to 3D for action detection in videos. Yu *et al.* [54] proposed a limited study on supervised skeleton-based action recognition using Capsule Network. Sankisa *et al.* [36] proposed to use Capsule Network for error concealment in videos.

Despite the success of capsule networks in various vision tasks, the study of capsule networks on motion representation is scarce. In this work, MCAE performs unsupervised learning of motion rep-

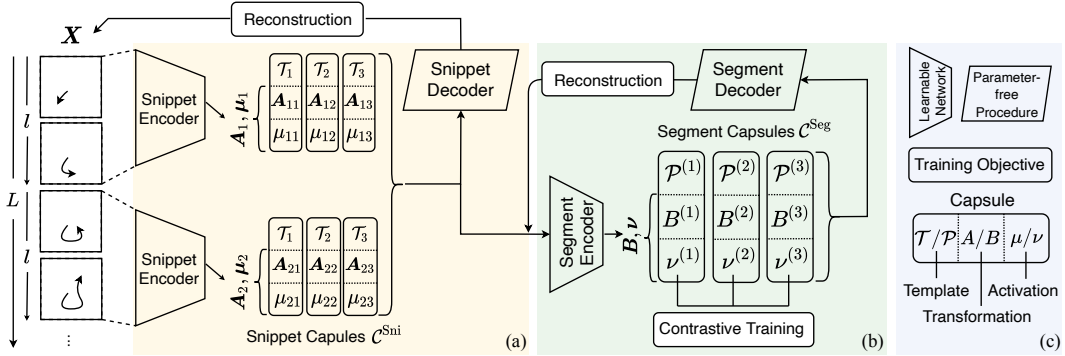


Figure 1: Overview of MCAE (best viewed in color). (a) The Snippet Autoencoder, which learns the semantic-agnostic short-time representation (snippet capsules) by reconstructing the input signal \mathbf{X} . (b) The Segment Autoencoder, which learns the semantic-aware long-time representation (segment capsules) by aggregating and reconstructing snippet capsule parameters. The activation values in segment capsules are used as semantic information for self-supervised contrastive training. (c) Meanings for different shapes and variables.

resented as coordinates rather than pixels. It aims at learning an appearance-agnostic transformation-invariant motion representation. We believe that introducing motion to the capsule network, or the other way round, provides (1) A new, robust, and efficient view into motion signals in any dimension space under the transformation-invariance assumption (while the motion and transformation in dimension space could have semantics different from their 2D/3D counterparts), and (2) proof that disentangling identity from transformation variance works not only for vision problems but a possibly larger family of time series analysis problems.

3 Methodology

We consider a single point¹ in d -dimension space. The motion of the point, i.e. a trajectory, is described by $\mathbf{X} = \{x_i | i = 1, \dots, L\}$, where $x_i \in \mathbb{R}^d$ is the coordinates at time i in a d -dimension space. Semantically, \mathbf{X} belongs to a motion pattern, subject to an arbitrary and unknown geometric transformation. Given sufficient samples of \mathbf{X} , we aim to learn a discriminative (in particular, transformation-invariant) representation for those motion samples without supervision.

3.1 Framework Overview

We solve this problem in two steps, namely *snippet learning* and *segment learning*. Snippets and segments correspond to the lower and higher levels of how MCAE views the motion signal. Both snippets and segments are temporally consecutive subsets of \mathbf{X} , but snippets have a shorter time span than segments. In the snippet learning step, the input \mathbf{X} is first divided into L/l temporally non-overlapping snippets, where l is the length of snippets. Each of these snippets will be mapped into a semantic-agnostic representation by the **Snippet Autoencoder**. In the segment learning step, the snippet representations are combined and fed into the **Segment Autoencoder**, where the full motion is represented as a weighted mixture of the transformed canonical representations. The segment activations are used as the motion representation for downstream tasks. An overview of the framework is shown in Fig. 1. In the following section, we delineate the details for each module and explain the training procedure.

3.2 Snippet Autoencoder

To encode the snippets' motion variation, we propose the Snippet Capsule (SniCap), which we denote as \mathcal{C}^{Sni} . SniCap is parameterized as $\mathcal{C}^{\text{Sni}} = \{\mathcal{T}, \mathcal{A}, \mu\}$, where \mathcal{T} , \mathcal{A} , and μ are the **snippet template**, **snippet transformation parameter**, and **snippet activation**, respectively. The snippet

¹We show a way to generalize MCAE to multi-point systems in Section 4.2

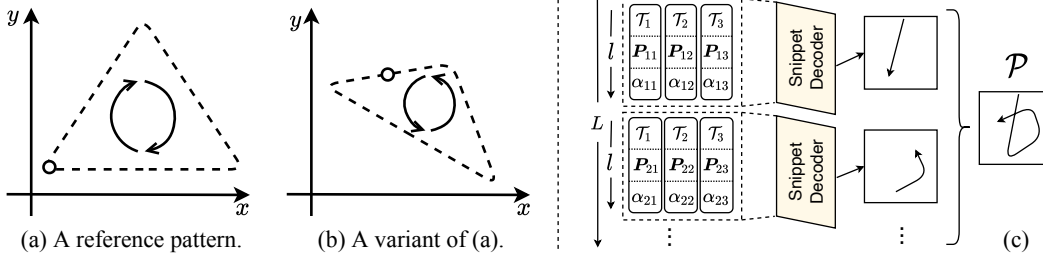


Figure 2: (a) and (b) show a reference motion pattern and a variant of it. The circle and the arrow shows the start and the direction of motion respectively. (c) Interpretation of a segment template \mathcal{P} . \mathcal{P} is functionally the same as S snippet parameters (\mathbf{A}, μ) . When combined with \mathcal{T} , it can be decoded into an L -long sequence. The segment autoencoder maintains multiple segment templates, which can be transformed and mixed to reconstruct the input snippet parameters.

template $\mathcal{T} = \{\mathbf{t}_i | \mathbf{t}_i \in \mathbb{R}^d, i = 1, \dots, l\}$ describes a motion template of length l and is the identity information of a SniCap. \mathbf{A} and μ depend on the input snippet. The transformation parameter $\mathbf{A} \in \mathbb{R}^{(d+1) \times (d+1)}$ describes the geometric relation between the input snippet and the snippet template. The snippet activation $\mu \in [0, 1]$ denotes whether the snippet template is activated to represent the input snippet.

Snippet Encoding/Decoding For a given snippet $\mathbf{x}_{i:i+l}$, the snippet module performs the following steps: (1) encode motion properties with Snippet Encoder into SniCaps, and (2) decode SniCaps to reconstruct the original $\mathbf{x}_{i:i+l}$. For the encoding step, a 1D-ConvNet f_{CONV} is used to extract the motion information from $\mathbf{x}_{i:i+l}$ and predict SniCap parameters, i.e. $\{(\mathbf{A}_j, \mu_j) | j = 1, \dots, N\} = f_{\text{CONV}}(\mathbf{x}_{i:i+l})$ where N is the number of SniCaps. The range of μ is confined by a sigmoid activation function. For the decoding step, we first apply the transformation \mathbf{A} to the snippet templates as

$$\begin{pmatrix} \hat{\mathbf{t}}_{ij} \\ 1 \end{pmatrix} = \mathbf{A}_i \begin{pmatrix} \mathbf{t}_j \\ 1 \end{pmatrix}, \quad i = 1, \dots, N, \quad j = 1, \dots, l. \quad (1)$$

Then, the transformed templates from different SniCaps are mixed, according to their activations, and the corresponding reconstructed input is

$$\hat{\mathbf{x}}_j = \sum_{i=1}^N \mu_i \hat{\mathbf{t}}_{ij}, \quad j = 1, \dots, l, \quad (2)$$

where $\hat{\mathbf{t}}_{ij}$ indicates the transformed coordinate of the i^{th} SniCap at j^{th} time step.

3.3 Segment Autoencoder

The motion information encoded in SniCaps is agnostic to the segment level motion patterns. This makes it less biased towards the training data domain. However, its utility on high-level applications, such as activity analysis or motion classification, is greatly undermined. For example, consider Fig. 2(a) as a reference “triangle” trajectory. Fig. 2(b) illustrates a possible intra-class variation. Since the two trajectories differ greatly in their local movement, they could be considered as different classes without transformation-invariant information from the full trajectory.

Hence, we introduce a segment encoder to gain a holistic understanding of motion and encapsulate such information in the segment capsules (SegCap). A segment is a motion of length L and can be interpreted as $S = L/l$ consecutive non-overlapping snippets. A SegCap is parameterized as $\mathcal{C}^{\text{Seg}} = \{\mathcal{P}, \mathbf{B}, \nu\}$, where \mathcal{P} , \mathbf{B} , and ν are the **segment template**, **segment transformation parameter**, and **segment activation**, respectively.

Different from the SniCap, whose template is explicitly a motion sequence, the SegCap parameterizes the segment template \mathcal{P} in terms of the N snippet templates. Specifically, $\mathcal{P} = \{(\mathbf{P}_i, \alpha_i) | i = 1, \dots, S\}$, where $\mathbf{P}_i \in \mathbb{R}^{N \times (d+1) \times (d+1)}$ and $\alpha_i \in \mathbb{R}^N$. Each $\mathbf{P}_{ij} \in \mathbb{R}^{(d+1) \times (d+1)}$ ($j \in [N]$ additionally indexes the first dimension of \mathbf{P}_i) describes how the j^{th} snippet template is aligned to form the i^{th} snippet of the segment template. The weight α_{ij} ($j \in [N]$ additionally indexes the elements of α_i)

controls the importance of j^{th} snippet template for the i^{th} snippet of the segment template. In other words, $(\mathbf{P}_i, \boldsymbol{\alpha}_i)$ describes how the N snippet templates are used to construct an l -long snippet and a SegCap requires S such parameters to describe an L -long segment template. Fig. 2(c) illustrates the interpretation of \mathcal{P} . \mathbf{B} and ν are dependent on the input. $\mathbf{B} \in \mathbb{R}^{(d+1) \times (d+1)}$ is a transformation on \mathbf{P} , and $\nu \in [0, 1]$ is the activation of the SegCap. The segment template \mathcal{P} is fixed for a SegCap w.r.t the training domain.

Segment Encoding/Decoding Assume we have M SegCaps with which we hope to reconstruct the low-level motion encoded in the SniCap parameters. This is equivalent to reconstructing all the data-dependent SniCap parameters $[\mathcal{C}_1^{\text{Sni}}, \dots, \mathcal{C}_S^{\text{Sni}}]$, where $\mathcal{C}_i^{\text{Sni}} = \{(\mathbf{A}_{ij}, \mu_{ij}) \mid j = 1, \dots, N\}$ is the set of SniCap parameters for the i^{th} snippet. To obtain the SegCap parameters, we first flatten each SniCap’s \mathbf{A} into a vector and concatenate it with its corresponding μ . Then we encode the S -long sequence of flattened SniCap parameters with an LSTM model f_{LSTM} shared by all SegCaps, and M fully-connected layers (one for each SegCap) to produce $\{\mathbf{B}, \nu\}$. Formally,

$$\begin{aligned} \mathbf{h} &= f_{\text{LSTM}}\left([\mathcal{C}_1^{\text{Sni}}, \dots, \mathcal{C}_S^{\text{Sni}}]\right), \\ \{\mathbf{B}^{(k)}, \nu^{(k)}\} &= f_{\text{FC}}^{(k)}(\mathbf{T}, \mathbf{h}), \quad k = 1, \dots, M, \end{aligned} \quad (3)$$

where $\mathbf{T} = \{\mathcal{T}_i \mid i = 1, \dots, N\}$, and superscript (k) refers to the k^{th} SegCap. The transformation and activation parameters are then applied to \mathcal{P} to reconstruct snippet parameters

$$\begin{aligned} \hat{\mathbf{P}}_{ij}^{(k)} &= \mathbf{B}^{(k)} \times \mathbf{P}_{ij}^{(k)}, \quad i = 1, \dots, S, \quad j = 1, \dots, N, \quad k = 1, \dots, M, \\ \hat{\mathcal{C}}_i^{\text{Sni}} &= (\hat{\mathbf{A}}_i, \hat{\boldsymbol{\mu}}_i) = \left(\sum_{k=1}^M \nu^{(k)} \hat{\mathbf{P}}_i^{(k)}, \sum_{k=1}^M \nu^{(k)} \boldsymbol{\alpha}_i^{(k)} \right), \quad i = 1, \dots, S, \end{aligned} \quad (4)$$

where $\hat{\mathbf{A}}_i \in \mathbb{R}^{N \times (d+1) \times (d+1)}$ and $\hat{\boldsymbol{\mu}}_i \in \mathbb{R}^N$ are the reconstructed snippet transformation and activation of the snippet templates for the i^{th} snippet. Note that $S = L/l$, which means f_{LSTM} can have a much smaller footprint than a recurrent network that handles the whole L -long sequence.

The above formulation enables SegCap to learn a transformation-invariant representation of motion. Intuitively, \mathcal{P} describes snippet-segment relation, and \mathbf{B} can be regarded as the spatial relation between a segment template pattern and the observed trajectory. The segment activation $\nu \in \mathbb{R}^M$ reveals the semantics of the input trajectory and can be used for self-supervised training.

3.4 Training

As delineated in Section 3.2 and 3.3, SniCap and SegCap play different roles by capturing information at two different abstraction levels. SniCap focuses on short-time motion while SegCap is defined upon SniCap to model long-time semantic information. Hence, the two autoencoders are trained using different objective functions.

The only objective of the snippet autoencoder is to faithfully reconstruct the original input. Therefore, for a training sample $\mathbf{X} = \{\mathbf{x}_i \mid i = 1, \dots, L\}$, we use a self-supervised reconstruction loss:

$$\mathcal{L}_{\text{Rec}}^{\text{Sni}} = \sum_{i=1}^L \|\hat{\mathbf{x}}_i - \mathbf{x}_i\|_2^2, \quad (5)$$

where $\hat{\mathbf{x}}_i$ denotes the reconstructed coordinate following Equation (2).

The segment autoencoder’s primary goal is to reconstruct the input SniCap parameters, hence the reconstruction loss

$$\mathcal{L}_{\text{Rec}}^{\text{Seg}} = \sum_{i=1}^S \|\hat{\mathbf{A}}_i - \mathbf{A}_i\|_2^2 + \|\hat{\boldsymbol{\mu}}_i - \boldsymbol{\mu}_i\|_2^2. \quad (6)$$

Furthermore, we use unsupervised contrastive training to learn semantic meaningful activations ν . For a batch of B samples, the contrastive loss is

$$\mathcal{L}_{\text{Con}}^{\text{Seg}} = -\frac{1}{B} \sum_{i=1}^B \log \frac{\exp(\text{cossim}(\boldsymbol{\nu}'_i, \boldsymbol{\nu}''_i)/\tau)}{\sum_{j=1, j \neq i}^B \exp(\text{cossim}(\boldsymbol{\nu}'_i, \boldsymbol{\nu}''_j)/\tau)}, \quad (7)$$

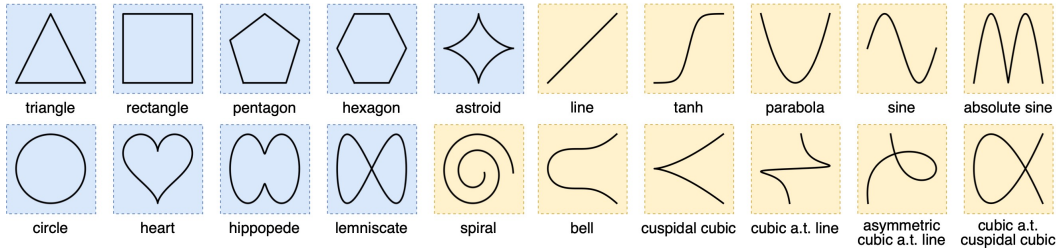


Figure 3: The 20 motion patterns in the Trajectory20 (T20) dataset. a.t. is short for “asymptotic to”.

where $\tau = 0.1$ is the temperature used for all experiments, ν'_i and ν''_i is the segment activation of sample \mathbf{X}'_i and \mathbf{X}''_i , respectively. Here, \mathbf{X}'_i and \mathbf{X}''_i are the spatial-temporally disturbed versions of \mathbf{X}_i . The disturbance is dataset-dependent and will be discussed in the appendix.

In addition to the above loss terms, we impose two regularizers: a smoothness constraint on reconstructed sequence, and a sparsity regularization on the segment activations

$$\mathcal{L}_{\text{Smt}}^{\text{Reg}} = \sum_{i=2}^L \|\hat{\mathbf{x}}_i - \hat{\mathbf{x}}_{i-1}\|_2^2, \quad \mathcal{L}_{\text{Sps}}^{\text{Reg}} = \|\nu\|_2^2. \quad (8)$$

The final training objective is:

$$\mathcal{L} = \lambda^{\text{Sni}} \mathcal{L}_{\text{Rec}}^{\text{Sni}} + \lambda^{\text{Seg}} \mathcal{L}_{\text{Rec}}^{\text{Seg}} + \mathcal{L}_{\text{Con}}^{\text{Seg}} + 0.5 \mathcal{L}_{\text{Smt}}^{\text{Reg}} + 0.05 \mathcal{L}_{\text{Sps}}^{\text{Reg}}, \quad (9)$$

where λ^{Sni} and λ^{Seg} are empirically determined.

4 Experiments

In this section, we first assess the proposed MCAE on a synthetic motion dataset to show its ability in learning transformation-invariant robust representations. Then, we generalize MCAE to multi-point systems and show its efficacy on real-world skeleton-based human action datasets. All unsupervised accuracies are produced by an auxiliary linear classifier that is trained on the motion representation learned by MCAE or the baselines, but whose gradient is blocked from back-propagating to the model. We report the mean accuracy and standard error based on three runs with random initialization. The experiments are run on an NVIDIA Titan V GPU, where we use a batch size of 64, and the Adam [16] optimizer with a learning rate of 10^{-3} . Please refer to the appendix for details.

4.1 Learning from Synthesized Motion

The Trajectory20 Dataset Although commonly used in the motion representation learning literature, datasets like movingMNIST [40] are innately *linear* and have limited motion variations. Moreover, the prediction-oriented setting makes it difficult to examine the motion category of each trajectory. In this paper, we introduce the Trajectory20 (T20), a synthetic trajectory dataset based on 20 distinct motion patterns (as shown in Fig. 3). Each sample in T20 is a 32-step-long sequence of coordinates in $[-1, 1]^2$. In the data generating process, a motion template is randomly picked, randomly rotated and scaled, and translated to a random position to produce a trajectory. A closed trajectory (marked blue in Fig. 3) starts at a random point on the trajectory and end at the same point, whereas an open trajectory (marked yellow in Fig. 3) starts at an either end’s vicinity. The randomized generating process ensures the trajectories are controllably diverse in scale, rotation, and position. The training data is generated on-the-fly and a fixed test set of 10,000 samples is used for evaluation. Examples of T20 are shown in the appendix.

Ablation Study We perform an ablation study of MCAE on T20 to examine the effect of different regularizers and three key hyperparameters: snippet length l , the numbers of SniCap (#Sni) and SegCap (#Seg). The result is shown in Table 1. The length of snippet l plays a vital role in learning a useful representation. A very small l results in a narrow receptive field for snippet capsules, which makes it less useful for inferring semantics of the whole sequence.

At the other end, a large l makes snippets challenging to reconstruct. The numbers of SniCap and SegCap also have major effect on the outcome. Too few SniCaps makes it difficult to reconstruct the input motion signal. Too few SegCaps undermines the expressiveness of the segment autoencoder. Too many SniCaps could cause difficulty in learning proper alignments between SegCaps and SniCaps. Both degrade the quality of the learned features. Moreover, increasing #Seg from 80 to 128 does not bring further improvements. As the result shows, $(l, \text{\#Sni}, \text{\#Seg}) = (8, 8, 80)$ performs well and we will use it in all experiments below. As for the regularizers, while both regularizers improve the performance, the sparsity regulation ($\mathcal{L}_{\text{Sps}}^{\text{Reg}}$) on segment activation is more helpful for learning discriminative features.

Table 1: Ablation study on T20.

Reg.	l	#Sni	#Seg	Acc. (%)
Full	8	8	80	69.30 ± 0.76
	4	8	80	41.01 ± 8.81
	16	8	80	45.83 ± 8.36
	8	2	80	64.02 ± 2.10
	8	4	80	68.17 ± 0.36
	8	16	80	48.11 ± 1.60
	8	8	32	42.36 ± 3.15
	8	8	64	63.94 ± 1.41
	8	8	128	69.44 ± 1.69
w/o $\mathcal{L}_{\text{Smt}}^{\text{Reg}}$	8	8	80	67.60 ± 1.69
w/o $\mathcal{L}_{\text{Sps}}^{\text{Reg}}$	8	8	80	65.92 ± 1.63

Motion Classification We compare MCAE with the following baseline models, namely KMeans, DTW-KMeans, k -Shape [31], LSTM and 1D-Conv². KMeans, DTW-KMeans, and k -Shape are parameter-free time series clustering algorithms. Briefly, KMeans uses Euclidean distance to measure the similarity between signals. DTW-KMeans normalizes input signals using dynamic time warping [35], and performs KMeans on the normalized signals. k -Shape uses cross-correlation based distance measure to cluster time series. We use the implementation by `tslearn` [42] for the three clustering methods. LSTM, 1D-Conv, and MCAE are used as backbone networks, which take the raw coordinate sequence as input and output a feature vector of a pre-defined dimension. The feature vector is used for contrastive learning following Equation (7). The corresponding accuracy reflects the quality of the learned representation.

For LSTM and 1D-Conv backbone, different numbers of hidden units/channels have been explored (shown as Hidden Param. in Table 2), which has resulted in different model sizes (measured by #Param. in Table 2).

As shown in Table 2, since the spatial variance (e.g. viewpoint changes) within motion signal cannot be directly captured by temporal warping/correlation, all the three parameter-free clustering methods perform poorly on T20. On the other hand, with considerably fewer parameters, MCAE outperforms LSTM and 1D-CNN by a large margin. This provides quantitative evidence that MCAE can capture the transformation-invariant semantic information more efficiently than the compared baselines.

Table 2: Unsupervised learning performance of MCAE and baselines on T20.

	Hidden Param.	#Param.	Acc. (%)
KMeans	–	–	8.57 ± 0.04
DTW-KMeans	–	–	9.12 ± 0.20
k -Shape [31]	–	–	12.94 ± 0.34
LSTM	128	600k	29.17 ± 2.45
	256	669k	40.03 ± 0.57
	512	805k	45.59 ± 1.37
	1,024	1,078k	53.47 ± 1.52
	2,048	1,625k	54.32 ± 0.55
1D-Conv	128	588k	44.78 ± 0.57
	256	787k	53.69 ± 0.53
	512	1,185k	57.57 ± 0.56
	1,024	1,982k	57.58 ± 0.08
	(#Sni, #Seg)	#Param.	Acc. (%)
MCAE	(8, 80)	277k	69.30 ± 0.76

4.2 Generalizing to Multiple Points

The MCAE running on T20 dataset handles a single moving point while most real-world problems involve multiple points. This section presents a naive (yet effective) extension of MCAE, which we name MCAE-MP, to enable processing motion for multi-point systems. Such motion can be described as $\mathcal{X} = \{\mathbf{X}_i | i = 1, \dots, K\}$, where K is the number of moving points. The extension works as follows:

²Architectures of LSTM and 1D-Conv are detailed in the supplementary material.

Table 3: Performance (%) for skeleton-based action classification. Column “Mod.” shows the data modality, where “S” indicates skeleton and “D” indicates depth map. Column “Cls.” shows the auxiliary classifier used for supervised training. We also report supervised SOTAs for completeness.

	Model	Mod.	Cls.	NTU60		NTU120		NW-UCLA
				XSUB	XVIEW	XSUB	XSET	V1&V2 → V3
Unsupervised	Luo <i>et al.</i> [27]	S+D	SLP	61.4	53.2	–	–	50.7
	Li <i>et al.</i> [20]	S+D	SLP	68.1	63.9	–	–	62.5
	SeBiReNet [29]	S	LSTM	–	79.7	–	–	80.3
	LongT GAN [62]	S	SLP	39.1	48.1	–	–	74.3
	MS ² L [24]	S	SLP	52.6	–	–	–	76.8
	CAE+ [33]	S	SLP	58.5	64.8	48.6	49.2	–
	MCAE-MP (SLP)	S	SLP	65.6	74.7	52.8	54.7	83.6
	P&C [41]	S	1-NN	50.7	76.1	–	–	84.9
MCAE-MP (1-NN)	S	1-NN	51.9	82.4	42.3	46.1	79.1	
Supv.	DropGraph [2]	S	–	90.5	96.6	82.4	84.3	93.8
	JOLO-GCN [1]	S	–	93.8	98.1	87.6	89.7	–

1. The K moving points are processed separately by an MCAE. This results in K segment activation vectors $\{\nu_i, |i = 1, \dots, K\}$.
2. The K activation vectors are concatenated into a single representation $\nu \in \mathbb{R}^{KM}$, which is used for unsupervised learning following Equation (9).

Skeleton-based Human Action Recognition We apply MCAE-MP to solve the unsupervised skeleton-based action recognition problem, where a human skeleton is a system consisting of multiple moving joints (points). Three widely-used datasets are used for evaluation: NW-UCLA [48], NTU-RGBD60 (NTU60) [37], and NTU-RGBD120 (NTU120) [25]. The three datasets consist of sequences with 1 or 2 subjects whose movement is measured in 3D space. For NW-UCLA, we follow previous works [41] to train the model on view 1 and 2, and test the model on view 3. For NTU60, we follow the official data split for the cross-subject (XSUB) and cross-view (XVIEW) protocols. The similar is implemented on NTU120 for the cross-subject (XSUB) and cross-setting (XSET) protocol. For ease of implementation, we project the 3D sequence into three orthonormal 2D spaces and use an MCAE defined on the 2D space to process the three views of the sequences. Then the segment activations from the three views are concatenated to form the representation. Four types of disturbance are introduced for contrastive learning, namely jittering, spatial rotation, masking, and temporal smoothing. The readers are referred to the appendix for details.

The classification accuracy is put into three groups in Table 3. In the first group are the prior works that are not directly comparable as they use depth map [27, 20] or stronger auxiliary classifiers for supervised training [29]. In the second group, where our model is marked as MCAE-MP (SLP), a single layer perceptron (SLP) is trained as the auxiliary classifier with backbone parameters frozen. In the third group, where our model is marked as MCAE-MP (1NN), a 1-nearest-neighbor classifier is used instead of an SLP. For completeness, the fourth group shows state-of-the-art results from supervised methods. Although MCAE-MP is a naive extension as it encodes joints separately and largely ignores their interactions, it achieves better or competitive performance compared with the baselines. Notably, on NTU60-XVIEW and NTU120-XSET where the training set and test set have different viewpoints, our model outperforms baselines by a clear margin thanks to the capsule-based representation which effectively captures viewpoint changes as transformations on input.

4.3 What does MCAE Learn?

To better understand what is encoded, we plot the learned snippet templates \mathcal{T} and segment templates \mathcal{P} in Fig. 4. Note that \mathcal{T} are initialized as random straight lines, and \mathcal{P} are initialized as arbitrary patterns composed randomly of \mathcal{T} . As shown in Fig. 4a, the snippets are mainly simple lines and hook-like curves that does not carry semantic information. Segment templates in Fig. 4b, however, bear some resemblance to the patterns shown in Fig. 3. This suggests that semantic-agnostic snippets are being aggregated into semantic-aware segments.

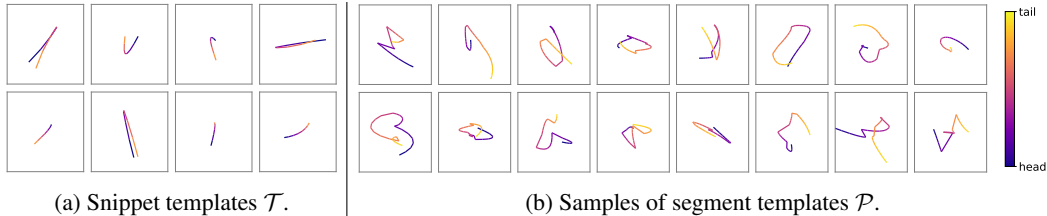


Figure 4: Templates learned from Trajectory20 dataset. Color indicates time.

Table 4: Top-5 segment templates (sorted by segment activation ν then segment ID for better visualization), and the rotation ϕ calculated from their parameters \mathbf{B} . Bold IDs are segments repeating across different θ .

Input	$\theta = -10^\circ$		$\theta = -5^\circ$		$\theta = 0^\circ$		$\theta = 5^\circ$		$\theta = 10^\circ$	
	ID	ϕ	ID	ϕ	ID	ϕ	ID	ϕ	ID	ϕ
hexagon	2	6.3	2	6.7	2	6.8	2	7.0	2	7.1
	8	6.9	8	9.0	8	11.2	8	13.9	8	16.5
	12	54.9	12	55.5	12	55.8	12	56.5	12	56.8
	37	-20.8	37	-19.8	37	-18.9	37	-17.9	37	-16.9
	66	50.2	66	52.5	66	55.4	66	59.0	66	62.4
abs_sine	2	12.1	2	12.3	2	12.2	2	12.1	2	11.9
	7	8.2	5	-10.7	5	-10.1	5	-9.9	7	17.2
	33	65.1	7	10.7	7	13.4	7	15.4	32	-9.7
	37	-22.9	37	-22.3	37	-21.8	37	-21.3	37	-19.9
	46	45.7	46	47.5	46	48.6	46	50.2	46	51.6

Table 5: Top-5 segment templates (sorted by segment activation ν then segment ID for better visualization), and the translation (x, y) calculated from their parameters \mathbf{B} .

Input	$(\Delta x, \Delta y) = (-0.2, 0)$			$(\Delta x, \Delta y) = (-0.1, 0)$			$(\Delta x, \Delta y) = (0, 0)$			$(\Delta x, \Delta y) = (0, 0.1)$			$(\Delta x, \Delta y) = (0, 0.2)$		
	ID	x	y	ID	x	y	ID	x	y	ID	x	y	ID	x	y
hexagon	2	0.05	0.18	2	0.17	0.19	2	0.27	0.19	2	0.28	0.28	2	0.27	0.37
	8	0.01	-0.07	8	0.09	-0.06	8	0.18	-0.04	8	0.19	0.04	8	0.19	0.12
	12	-0.09	0.13	12	0.00	0.13	12	0.09	0.13	12	0.09	0.23	12	0.09	0.32
	37	0.10	-0.11	37	0.18	-0.11	37	0.27	-0.11	37	0.27	-0.03	37	0.27	0.05
	66	-0.12	0.16	66	-0.03	0.16	66	0.05	0.17	66	0.06	0.26	66	0.06	0.35
abs_sine	2	0.04	0.2	2	0.14	0.19	2	0.24	0.19	2	0.24	0.28	2	0.23	0.38
	5	-0.01	0.30	5	0.07	0.29	5	0.16	0.29	5	0.16	0.38	5	0.15	0.46
	7	0.20	-0.16	7	0.28	-0.16	7	0.37	-0.15	7	0.36	-0.06	7	0.36	0.04
	37	0.04	-0.17	37	0.12	-0.16	37	0.21	-0.16	37	0.20	-0.07	37	0.20	0.01
	46	0.02	0.01	46	0.13	0.02	46	0.23	0.04	46	0.23	0.13	46	0.22	0.23

We proceed to explore the information in SegCaps. In particular, we would like to see if SegCaps have learned transformation-invariant information. To this purpose, we randomly sample a trajectory from T20 dataset. The trajectory is first normalized so that its centroid is at $(0, 0)$, then rotated clockwise by an angle θ , and finally fed into the model. We examine the segment templates with the highest activation values (which reflects the trajectory’s semantics) and calculate the rotation angle ϕ from those templates’ parameter \mathbf{B} . As shown in Table 4, the calculated ϕ reveals two types of segments templates as we rotate the input. One type yields constant ϕ (e.g. segment ID 2 for sample “absolute sine”), which indicates its rotation-invariance, the other has ϕ that changes monotonically with θ (e.g. segment ID 8 for sample “hexagon”), which shows its rotation-awareness. As for the activation values, samples from different categories activate different sets of segment templates. Meanwhile, the same sample under different rotation angle θ gives stable segment template activations, despite some changes which are found to have no effect on the classification result.

We do a similar study on the translation component (x, y) , where we translate the input by $(\Delta x, \Delta y)$. As shown in Table 5, (x, y) changes monotonically with $(\Delta x, \Delta y)$ while the activated segment templates remain stable. These results prove that the semantics and transformation information has been encoded separately in the segment activation ν and transformation parameters \mathbf{B} . In other words, the encoded semantic information is robust against geometric transformations.

5 Conclusion

In this paper, we introduce MCAE, a framework that learns robust and discriminative representation for keypoint motion. To resolve the intra-class variation of motion, we propose to learn a compact and transformation-invariant motion representation using a two-level capsule-based representation hierarchy. The efficacy of the learned representation is shown through an experimental study on synthetic and real-world datasets. The output of MCAE could serve as mid-level representation in other frameworks, e.g. Graph Convolution Network, for tasks that involve more context than classification. We anticipate this work to inspire further studies that apply capsule-based models to other time series processing tasks, such as joint modeling of visual appearance and motion in video. The software and the T20 dataset of our research are accessible at <https://github.com/ZiweiXU/CapsuleMotion>.

Motion analysis techniques are in the foreground of the misuse of machine learning methods, among which adverse societal impacts and privacy breach are two major concerns. Regarding the societal impacts, admittedly, our method has both upside and downside. On one hand, a transformation-invariant motion representation enables us better decode the information implicit in the trajectory, which has applications for example in ethology. On the other hand, it could also be misused in mass surveillance. Appropriate boundaries of use and ethical review are required to prevent potential malicious applications. Regarding the privacy concerns, our method isolates the subjects' motion from their sensitive information, such as gender and race.

Acknowledgments

This research/project is supported by the National Research Foundation, Singapore under its Strategic Capability Research Centres Funding Initiative. Any opinions, findings and conclusions or recommendations expressed in this material are those of the author(s) and do not reflect the views of National Research Foundation, Singapore. The computational work for this article was partially performed on resources of the National Supercomputing Centre, Singapore (<https://www.nscg.sg>).

References

- [1] Jinmiao Cai, Nianjuan Jiang, Xiaoguang Han, Kui Jia, and Jiangbo Lu. JOLO-GCN: mining joint-centered light-weight information for skeleton-based action recognition. In *WACV*, pages 2734–2743. IEEE, 2021.
- [2] Ke Cheng, Yifan Zhang, Congqi Cao, Lei Shi, Jian Cheng, and Hanqing Lu. Decoupling GCN with dropgraph module for skeleton-based action recognition. In *ECCV*, pages 536–553. Springer, 2020.
- [3] Jeff Donahue, Lisa Anne Hendricks, Marcus Rohrbach, Subhashini Venugopalan, Sergio Guadarrama, Kate Saenko, and Trevor Darrell. Long-term recurrent convolutional networks for visual recognition and description. *IEEE Transactions on Pattern Analysis and Machine Intelligence*, 39(4):677–691, 2017.
- [4] Yong Du, Wei Wang, and Liang Wang. Hierarchical recurrent neural network for skeleton based action recognition. In *CVPR*, pages 1110–1118, 2015.
- [5] Kevin Duarte, Yogesh Rawat, and Mubarak Shah. VideoCapsuleNet: A simplified network for action detection. In *NeurIPS*, pages 7610–7619, 2018.
- [6] Hehe Fan, Yi Yang, and Mohan Kankanhalli. Point 4d transformer networks for spatio-temporal modeling in point cloud videos. In *IEEE/CVF Conference on Computer Vision and Pattern Recognition*, 2021.
- [7] Hehe Fan, Xin Yu, Yuhang Ding, Yi Yang, and Mohan Kankanhalli. PSTNet: Point spatio-temporal convolution on point cloud sequences. In *International Conference on Learning Representations (ICLR)*, 2021.
- [8] Tian Gan, Yongkang Wong, Daqing Zhang, and Mohan Kankanhalli. Temporal encoded f-formation system for social interaction detection. In *ACM Multimedia*, pages 937–946, 2013.
- [9] Agrim Gupta, Justin Johnson, Li Fei-Fei, Silvio Savarese, and Alexandre Alahi. Social GAN: Socially acceptable trajectories with generative adversarial networks. In *CVPR*, pages 2255–2264, 2018.

- [10] Ahmed Refaat Hawas, Heba A. El-Khobby, Mohammed Abd-Elnaby, and Fathi E. Abd El-Samie. Gait identification by convolutional neural networks and optical flow. *Multimedia Tools and Applications*, 78(18):25873–25888, 2019.
- [11] Geoffrey E. Hinton, Alex Krizhevsky, and Sida D. Wang. Transforming auto-encoders. In *ICANN*, volume 6791 of *Lecture Notes in Computer Science*, pages 44–51. Springer, 2011.
- [12] Geoffrey E. Hinton, Sara Sabour, and Nicholas Frosst. Matrix capsules with EM routing. In *ICLR (Poster)*. OpenReview.net, 2018.
- [13] Noureldien Hussein, Efstratios Gavves, and Arnold W. M. Smeulders. Timeception for complex action recognition. In *CVPR*, pages 254–263. Computer Vision Foundation / IEEE, 2019.
- [14] Mariano Jaimez, Mohamed Souiai, Javier Gonzalez-Jimenez, and Daniel Cremers. A primal-dual framework for real-time dense RGB-D scene flow. In *ICRA*, pages 98–104, 2015.
- [15] Yanli Ji, Feixiang Xu, Yang Yang, Ning Xie, Heng Tao Shen, and Tatsuya Harada. Attention transfer (ANT) network for view-invariant action recognition. In *ACM Multimedia*, pages 574–582, 2019.
- [16] Diederik P. Kingma and Jimmy Ba. Adam: A method for stochastic optimization. In *ICLR*, 2015.
- [17] Adam Kosioerek, Sara Sabour, Yee Whye Teh, and Geoffrey E Hinton. Stacked capsule autoencoders. In *NeurIPS*, pages 15512–15522, 2019.
- [18] Mohamed Ilyes Lakhal, Oswald Lanz, and Andrea Cavallaro. View-1stm: Novel-view video synthesis through view decomposition. In *ICCV*, pages 7576–7586, 2019.
- [19] Binlong Li, Octavia I. Camps, and Mario Szaier. Cross-view activity recognition using hand-kelets. In *CVPR*, pages 1362–1369, 2012.
- [20] Junnan Li, Yongkang Wong, Qi Zhao, and Mohan S. Kankanhalli. Unsupervised learning of view-invariant action representations. In *NeurIPS*, pages 1262–1272, 2018.
- [21] Maosen Li, Siheng Chen, Xu Chen, Ya Zhang, Yanfeng Wang, and Qi Tian. Actional-structural graph convolutional networks for skeleton-based action recognition. In *CVPR*, pages 3595–3603, 2019.
- [22] Wanqing Li, Zhengyou Zhang, and Zicheng Liu. Action recognition based on a bag of 3D points. In *CVPR Workshops*, pages 9–14, 2010.
- [23] Yan Li, Bin Ji, Xintian Shi, Jianguo Zhang, Bin Kang, and Limin Wang. TEA: Temporal excitation and aggregation for action recognition. In *CVPR*, pages 906–915, 2020.
- [24] Lilang Lin, Sijie Song, Wenhan Yang, and Jiaying Liu. MS2L: multi-task self-supervised learning for skeleton based action recognition. In *ACM Multimedia*, pages 2490–2498, 2020.
- [25] Jun Liu, Amir Shahroudy, Mauricio Perez, Gang Wang, Ling-Yu Duan, and Alex C. Kot. NTU RGB+D 120: A large-scale benchmark for 3D human activity understanding. *IEEE Transaction on Pattern Analysis and Machine Intelligence*, 42(10):2684–2701, 2020.
- [26] Ziyu Liu, Hongwen Zhang, Zhenghao Chen, Zhiyong Wang, and Wanli Ouyang. Disentangling and unifying graph convolutions for skeleton-based action recognition. In *CVPR*, pages 143–152, 2020.
- [27] Zelun Luo, Boya Peng, De-An Huang, Alexandre Alahi, and Li Fei-Fei. Unsupervised learning of long-term motion dynamics for videos. In *CVPR*, pages 7101–7110. IEEE Computer Society, 2017.
- [28] Joe Yue-Hei Ng, Matthew J. Hausknecht, Sudheendra Vijayanarasimhan, Oriol Vinyals, Rajat Monga, and George Toderici. Beyond short snippets: Deep networks for video classification. In *CVPR*, pages 4694–4702, 2015.
- [29] Qiang Nie, Ziwei Liu, and Yunhui Liu. Unsupervised 3d human pose representation with viewpoint and pose disentanglement. In *ECCV*, volume 12364 of *Lecture Notes in Computer Science*, pages 102–118. Springer, 2020.
- [30] Dan Oneata, Jakob Verbeek, and Cordelia Schmid. Action and event recognition with fisher vectors on a compact feature set. In *ICCV*, pages 1817–1824, 2013.
- [31] John Paparrizos and Luis Gravano. k-shape: Efficient and accurate clustering of time series. In *SIGMOD*, pages 1855–1870, 2015.

- [32] Vasu Parameswaran and Rama Chellappa. View invariance for human action recognition. *International Journal of Computer Vision*, 66(1):83–101, 2006.
- [33] Haocong Rao, Shihao Xu, Xiping Hu, Jun Cheng, and Bin Hu. Augmented skeleton based contrastive action learning with momentum LSTM for unsupervised action recognition. *Information Sciences*, 569:90–109, August 2021.
- [34] Sara Sabour, Nicholas Frosst, and Geoffrey E Hinton. Dynamic routing between capsules. In *NIPS*, pages 3856–3866, 2017.
- [35] Hiroaki Sakoe and Seibi Chiba. Dynamic programming algorithm optimization for spoken word recognition. *IEEE Transactions on Acoustics, Speech, and Signal Processing*, 26(1):43–49, 1978.
- [36] Arun Sankisa, Arjun Punjabi, and Aggelos K. Katsaggelos. Temporal capsule networks for video motion estimation and error concealment. *Signal Image Video Process.*, 14(7):1369–1377, 2020.
- [37] Amir Shahroudy, Jun Liu, Tian-Tsong Ng, and Gang Wang. NTU RGB+D: A large scale dataset for 3D human activity analysis. In *CVPR*, pages 1010–1019, 2016.
- [38] Xingjian Shi, Zhoung Chen, Hao Wang, Dit-Yan Yeung, Wai-Kin Wong, and Wang-chun Woo. Convolutional LSTM network: A machine learning approach for precipitation nowcasting. In *NIPS*, pages 802–810, 2015.
- [39] Karen Simonyan and Andrew Zisserman. Two-stream convolutional networks for action recognition in videos. In *NIPS*, pages 568–576, 2014.
- [40] Nitish Srivastava, Elman Mansimov, and Ruslan Salakhutdinov. Unsupervised learning of video representations using LSTMs. In *ICML*, volume 37 of *JMLR Workshop and Conference Proceedings*, pages 843–852, 2015.
- [41] Kun Su, Xiulong Liu, and Eli Shlizerman. PREDICT & CLUSTER: unsupervised skeleton based action recognition. In *CVPR*, pages 9628–9637, 2020.
- [42] Romain Tavenard, Johann Faouzi, Gilles Vandewiele, Felix Divo, Guillaume Androz, Chester Holtz, Marie Payne, Roman Yurchak, Marc Rußwurm, Kushal Kolar, and Eli Woods. Tslern, a machine learning toolkit for time series data. *Journal of Machine Learning Research*, 21(118):1–6, 2020.
- [43] Du Tran, Lubomir Bourdev, Rob Fergus, Lorenzo Torresani, and Manohar Paluri. Learning spatiotemporal features with 3D convolutional networks. In *ICCV*, pages 4489–4497, 2015.
- [44] Raviteja Vemulapalli, Felipe Arrate, and Rama Chellappa. Human action recognition by representing 3D skeletons as points in a Lie group. In *CVPR*, pages 588–595, 2014.
- [45] Shruti Vyas, Yogesh Singh Rawat, and Mubarak Shah. Multi-view action recognition using cross-view video prediction. In *ECCV*, volume 12372 of *Lecture Notes in Computer Science*, pages 427–444. Springer, 2020.
- [46] Heng Wang and Cordelia Schmid. Action recognition with improved trajectories. In *ICCV*, pages 3551–3558, 2013.
- [47] Jiang Wang, Zicheng Liu, Ying Wu, and Junsong Yuan. Mining actionlet ensemble for action recognition with depth cameras. In *CVPR*, pages 1290–1297, 2012.
- [48] Jiang Wang, Xiaohan Nie, Yin Xia, Ying Wu, and Song-Chun Zhu. Cross-view action modeling, learning, and recognition. In *CVPR*, pages 2649–2656, 2014.
- [49] Limin Wang, Zhan Tong, Bin Ji, and Gangshan Wu. TDN: temporal difference networks for efficient action recognition. In *CVPR*, pages 1895–1904, 2021.
- [50] Xiaolong Wang, Ross Girshick, Abhinav Gupta, and Kaiming He. Non-local neural networks. In *CVPR*, pages 7794–7803, 2018.
- [51] Yunbo Wang, Lu Jiang, Ming-Hsuan Yang, Li-Jia Li, Mingsheng Long, and Li Fei-Fei. Eidetic 3D LSTM: A model for video prediction and beyond. In *ICLR*, 2019.
- [52] Sijie Yan, Yuanjun Xiong, and Dahua Lin. Spatial temporal graph convolutional networks for skeleton-based action recognition. In *AAAI*, 2018.
- [53] Ceyuan Yang, Yinghao Xu, Jianping Shi, Bo Dai, and Bolei Zhou. Temporal pyramid network for action recognition. In *CVPR*, pages 588–597, 2020.

- [54] Yue Yu, Niehao Tian, Xiangru Chen, and Ying Li. Skeleton capsule net: An efficient network for action recognition. In *ICVRV*, pages 74–77, 2018.
- [55] Pengfei Zhang, Cuiling Lan, Wenjun Zeng, Junliang Xing, Jianru Xue, and Nanning Zheng. Semantics-guided neural networks for efficient skeleton-based human action recognition. In *CVPR*, pages 1112–1121, 2020.
- [56] Shiwen Zhang, Sheng Guo, Weilin Huang, Matthew R. Scott, and Limin Wang. V4D: 4d convolutional neural networks for video-level representation learning. In *ICLR*, 2020.
- [57] Xikun Zhang, Chang Xu, and Dacheng Tao. Context aware graph convolution for skeleton-based action recognition. In *CVPR*, pages 14333–14342, 2020.
- [58] Yiyi Zhang, Li Niu, Ziqi Pan, Meichao Luo, Jianfu Zhang, Dawei Cheng, and Liqing Zhang. Exploiting motion information from unlabeled videos for static image action recognition. In *AAAI*, pages 12918–12925, 2020.
- [59] Yujia Zhang, Xiaodan Liang, Dingwen Zhang, Min Tan, and Eric P Xing. Unsupervised object-level video summarization with online motion auto-encoder. *Pattern Recognition Letters*, 130:376–385, 2020.
- [60] Yongheng Zhao, Tolga Birdal, Haowen Deng, and Federico Tombari. 3D point capsule networks. In *CVPR*, pages 1009–1018, 2019.
- [61] Yongheng Zhao, Tolga Birdal, Jan Eric Lenssen, Emanuele Menegatti, Leonidas J. Guibas, and Federico Tombari. Quaternion equivariant capsule networks for 3D point clouds. In *ECCV*, volume 12346 of *Lecture Notes in Computer Science*, pages 1–19. Springer, 2020.
- [62] Nenggan Zheng, Jun Wen, Risheng Liu, Liangqu Long, Jianhua Dai, and Zhefeng Gong. Unsupervised representation learning with long-term dynamics for skeleton based action recognition. In *AAAI*, pages 2644–2651, 2018.
- [63] Tao Zhuo, Zhiyong Cheng, Peng Zhang, Yongkang Wong, and Mohan Kankanhalli. Explainable video action reasoning via prior knowledge and state transitions. In *ACM Multimedia*, pages 521–529, 2019.

A Table of Notations

We show in the table below the notations grouped by the modules. The values used in our implementation are shown if applicable.

Table 6: Table of Notations

Model	
\mathbf{X}	Input motion signal
\mathbf{x}_t	The t^{th} time step of the input signal
Sizes	
$L = 32$	Input length
$l = 8$	Snippet length
S	Number of snippets, $S = L/l$
$N = 8$	Number of snippet capsules
$M = 80$	Number of segment capsules
Snippet Capsule	
SniCap	Snippet Capsule
\mathcal{T}	Snippet template (of a snippet capsule)
\mathbf{A}	Snippet transformation parameters
μ_i	Activation of the i^{th} snippet template
Segment Capsule	
SegCap	Segment Capsule
\mathcal{P}	Segment template (of a segment capsule)
\mathbf{P}	Spatial relation between a segment template and all the snippet templates
α	The weights of snippet templates when used to form a segment template
\mathbf{B}	Segment transformation parameters
$\nu^{(k)}$	Activation of the k^{th} segment template

B Number of Layers

Table 7: Performance of single and double layer model on T20 dataset of different lengths.

	$L = 32$	$L = 64$	$L = 128$	$L = 256$
Single	47.64 ± 1.68	28.43 ± 2.95	35.23 ± 1.38	31.42 ± 0.53
Double	69.30 ± 0.76	69.88 ± 3.53	66.45 ± 0.39	65.24 ± 6.62

The necessity of a two-layer hierarchy is briefly discussed in Section 3.3. In short, it is difficult for a single-layer hierarchy to capture long-time dependencies and variations. This section describes an empirical study where we compare MCAE with its single-layer correspondence. The single-layer model is an MCAE without the segment autoencoder and with an increased number of 80 snippet capsules. The snippet length l is set to input length L , and the snippet activations μ are used for contrastive learning. The double-layer model is the MCAE proposed in the paper. Both models are trained using samples from T20 interpolated to four different lengths $\{32, 64, 128, 256\}$. The results are shown in Table 7. The first observation is that the single-layer model performs poorly in all four configurations. More importantly, as L increases, the single-layer model degrades severely while the double-layer model performs well consistently.

C Implementation

Transformation Parameters The MCAE implementation in the main paper works in 2D spaces. To regulate the model, the snippet and segment encoders are set to output five parameters for each template: μ (or ν), s , t_x , t_y , and θ , where the first parameter is the activation and the last four

Table 8: Convolution backbone. When used in the snippet encoder, $C = 8$ and $D = 5N$. When used for 1D-Conv baseline, $C = 48$ and D is set to the number of hidden units. The Leaky ReLU has a negative slope of 0.01.

	Channels in	Channels out	Kernel Size	Stride	Padding
1D Conv Layer	2	C	4	2	1
Batch Normalization					
Leaky ReLU					
1D Conv Layer	C	$2C$	4	2	1
Batch Normalization					
Leaky ReLU					
1D Conv Layer	$2C$	$4C$	4	2	1
Batch Normalization					
Leaky ReLU					
1D Conv Layer	$4C$	D	1	1	0

parameters form a transformation as follows

$$\begin{pmatrix} \sigma(s) \cos \theta & -\sigma(s) \sin \theta & f(t_x, 1.5) \\ \sigma(s) \sin \theta & \sigma(s) \cos \theta & f(t_y, 1.5) \\ 0 & 0 & 1 \end{pmatrix}, \quad (10)$$

where $\sigma(\cdot)$ is the sigmoid function, and $f(x, t) = \max(-t, \min(x, t))$ ‘‘clamps’’ x within $[-t, t]$. The value $t = 1.5$ allows for more flexibility as the input is generally in $[-1, 1]$ in our experiments.

Snippet Encoder The 1D ConvNet f_{conv} in the snippet encoder is defined in Table 8, with $C = 8$ and $D = 5N$ where N is the number of snippet capsules, and the factor 5 corresponds to the five parameters for each capsule $\{\mu, s, t_x, t_y, \theta\}$. The $5N$ -dimension output is used as transformation parameters for snippet capsules.

Segment Encoder The f_{LSTM} in the segment encoder is a bi-directional LSTM (BiLSTM) with 32 hidden units. The 64-dimension hidden state of f_{LSTM} at the last time step is sent to a fully connected layer which gives $32M$ -dimension output. It is then fed into M different fully connected layers, each of which outputs five parameters for a segment capsule.

Baselines The 1D-Conv baseline uses the same architecture as f_{conv} , which is defined in Table 8. To improve its performance, we use $C = 48$ and experimented with a variable D as hidden unit numbers. The LSTM baseline is a BiLSTM with 256 hidden units. Its 512-dimension output is fed to a fully connected layer with a variable output dimension D , whose output is activated by a leaky ReLU function. Different values of D have been explored in the main paper.

D Training Details

Hyperparameters We set the batch size to 64 and use a fixed learning rate 10^{-3} . The models are optimized using the Adam [16] optimizer. The training stops when the model’s performance stagnates for over 100 epochs or right after the 1000^{th} epoch, whichever is earlier. For experiments on T20, we set the random seed to 0, 1, and 2. For experiments on NW-UCLA, NTURGBD60, and NTURGBD120, we set random seed 0. There is no tuning of random seeds. The loss weights λ^{Sni} and λ^{Seg} are searched in $\{0.5, 1, 1.5, 2, 5, 10\}$. For T20 and NW-UCLA, we use $\lambda^{\text{Sni}} = \lambda^{\text{Seg}} = 1$. For NTURGBD60 and NTURGBD120, we use $\lambda^{\text{Sni}} = 10$ and $\lambda^{\text{Seg}} = 5$.

Software and Hardware All the models are implemented using PyTorch 1.8 compiled with CUDA 11.2 and CuDNN 7.6.5. The computation runs on an NVIDIA Titan V GPU with 12GB memory. The typical time required for experiments on T20, NW-UCLA, NTURGBD60, and NTURGBD120 is 7hrs, 0.5hrs, 6hrs, and 16hrs, respectively.

Contrastive Learning We use four disturbance (data augmentation) methods in the experiments:

Table 9: Examples of the Trajectory20 dataset (a.t. is short for “asymptotic to”).

Triangle	Rectangle	Pentagon	Hexagon	Astroid	Circle	Heart	Hippopede	Lemniscate	Spiral
Line	Tanh	Parabola	Sine	Absolute Sine	Bell	Cuspidal Cubic	Cubic a.t. Line	Asymmetric Cubic a.t. Line	Cubic a.t. Cuspidal Cubic

1. **Rotate:** Applied to T20 and skeleton datasets. For T20 dataset, the input is rotated by a random angle between -30° and 30° . For skeleton datasets, the orientation for rotation is randomly determined from yaw, pitch, or roll.
2. **Smooth:** Applied to T20 and skeleton datasets. The input sequences are temporally filtered by a moving average kernel of size 3.
3. **Jittering:** Applied to skeleton datasets only. A random number $m \sim U(0, 1)$ is sampled for each joint. The coordinates of a joint are disturbed by Gaussian noise $n \sim \mathcal{N}(0, 1)$ in all the time steps if $m < 0.1$ and kept unchanged otherwise.
4. **Masking:** Applied to skeleton datasets only. A random number $m \sim U(0, 1)$ is sampled for each joint. The coordinates of a joint are masked by 0 in all the time steps if $m < 0.2$ and kept unchanged otherwise.

The disturbance methods applied for each training sample are randomly determined.

E Examples of the Trajectory20 (T20) dataset

We show in Table 9 some examples of the T20 dataset. The color gradient from blue to yellow indicates the time steps. For closed trajectories, the point moves in a randomly selected direction and finishes one whole trajectory. For open trajectories, the point starts at one end in a randomly selected direction and finishes at the other end.